AD-A105 784 AEROSPACE CORP EL SEGUNDO CA SPACE SCIENCES LAB F/G 8/7
SATELLITE OBSERVATIONS OF THE MT. ST. HELENS ERUPTION OF 18 MAY--ETC(U)
AUG 81 C J RICE F04701-80-C-0081
UNCLASSIFIED TR-0081(6640)-3 SD-TR-81-70 NL

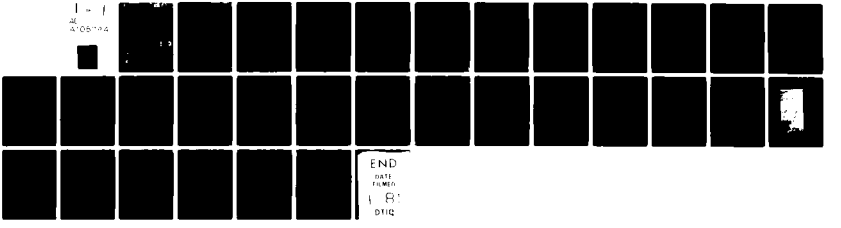

Satellite Observations of the Mt. St. Helens Eruption of 18 May 1980

Prepared by

C. J. RICE
Space Sciences Laboratory
Laboratory Operations
The Aerospace Corporation
El Segundo, Calif. 90245

21 August 1981

Prepared for

AIR FORCE TECHNICAL APPLICATIONS CENTER
Patrick Air Force Base, Fla. 31935

SPACE DIVISION
AIR FORCE SYSTEMS COMMAND
Los Angeles Air Force Station
P.O. Box 91960, Worldway Postal Center
Los Angeles, Calif. 90009

This report was submitted by The Aerospace Corporation, El Segundo, CA 90245, under Contract No. F04701-80-C-0081 with the Space Division, Deputy for Technology, P.O. Box 92960, Worldway Postal Center, Los Angeles, CA 90009. It was reviewed and approved for The Aerospace Corporation by G. A. Paulikas, Acting Director, Space Sciences Laboratory. Lt. J. C. Garcia, SD/YLVS, was the project officer for Technology.

This report has been reviewed by the Public Affairs Office (PAS) and is releasable to the National Technical Information Service (NTIS). At NTIS, it will be available to the general public, *including foreign nations.*

This technical report has been reviewed and is approved for publication. Publication of this report does not constitute Air Force approval of the report's findings or conclusions. It is published only for the exchange and stimulation of ideas.

James C. Garcia, 1st Lt, USAF
Project Officer

Florian P. Meinhardt, Lt Col, USAF
Director, Directorate of Advanced
Space Development

FOR THE COMMANDER

Norman W. Lee, Jr., Colonel, USAF
Deputy for Technology

UNCLASSIFIED

SECURITY CLASSIFICATION OF THIS PAGE (When Data Entered)

REPORT DOCUMENTATION PAGE

READ INSTRUCTIONS BEFORE COMPLETING FORM

1. REPORT NUMBER: SD-TR-81-76	2. GOVT ACCESSION NO.: ADA105784
3. RECIPIENT'S CATALOG NUMBER:	
4. TITLE (and Subtitle): SATELLITE OBSERVATIONS OF THE MT. ST. HELENS ERUPTION OF 18 MAY 1980	5. TYPE OF REPORT & PERIOD COVERED:
	6. PERFORMING ORG. REPORT NUMBER: TR-0081(6640)-3
7. AUTHOR(s): Carl J. Rice	8. CONTRACT OR GRANT NUMBER(s): F04701-80-C-0081
9. PERFORMING ORGANIZATION NAME AND ADDRESS: The Aerospace Corporation, El Segundo, Calif. 90245	10. PROGRAM ELEMENT, PROJECT, TASK AREA & WORK UNIT NUMBERS: 62
11. CONTROLLING OFFICE NAME AND ADDRESS: Air Force Technical Applications Center, Patrick Air Force Base, Fla. 31935	12. REPORT DATE: 21 August 1981 13. NUMBER OF PAGES: 31
14. MONITORING AGENCY NAME & ADDRESS (if different from Controlling Office): Space Division, Air Force Systems Command	15. SECURITY CLASS. (of this report): Unclassified 15a. DECLASSIFICATION/DOWNGRADING SCHEDULE:

16. DISTRIBUTION STATEMENT (of this Report)

Approved for public release; distribution unlimited

17. DISTRIBUTION STATEMENT (of the abstract entered in Block 20, if different from Report)

18. SUPPLEMENTARY NOTES

19. KEY WORDS (Continue on reverse side if necessary and identify by block number)

Cascades Volcanoes
18 May 1980 Eruption of Mt. St. Helens
Eruption Chronology
Infrared Observations
Mt. St. Helens
Satellite Observations
Volcanic Eruptions

20. ABSTRACT (Continue on reverse side if necessary and identify by block number)

The explosive eruption of Mt. St. Helens on 18 May 1980 was monitored by infrared sensors aboard two U.S. Air Force satellites. Essentially continuous data are available following the initial sighting of the eruption cloud less than one minute after the earthquake which triggered the eruption. Dual monitoring permits triangulation so that both the horizontal and vertical development of the eruption can be determined with good temporal resolution. The sequence of events occurring early in the eruption can therefore be established.

DD FORM (FACSIMILE) 1473

UNCLASSIFIED

SECURITY CLASSIFICATION OF THIS PAGE (When Data Entered)

PREFACE

The interest and support of many people have made this research possible. Particular thanks are given to those individuals who helped to obtain the data. This work was supported in part by the Aerospace-Sponsored Research Program and in part by the U. S. Air Force Space Division under Contract F04701-80-C-0081.

CONTENTS

FIGURES

TABLE

INTRODUCTION

The eruption of Mt. St. Helens on 18 May 1980 was observed by many ground observers. The eyewitness accounts and snapshot sequences made by these people have elucidated many aspects of the series of events which occurred, particularly during the landslide and initial ash emissions. While controls on the timing of the photographs are missing, the study of certain features in successive frames can permit establishing a reasonable relative timing. Because of their proximity, however, the witnesses were very quickly overwhelmed by the developing ash cloud after which photography was not possible. Photographs made at greater distances show less detail, of course, and also lack critical timing controls.

The eruption was also detected by numerous sensors in space. Images were obtained by the Geostationary Operational Environmental Satellites (GOES), NOAA-6, and the U.S. Air Force weather satellite DMSP. The photographs from GOES-West have been particularly widely circulated and studied. However, even the earliest of these, the GOES-West visible photograph made at 15:45 UT (Universal or Greenwich Mean Time, equal to 8:45 A.M., Pacific Daylight Time - all times quoted in this report will use Universal Time) shows the eruption some 12-13 minutes after its beginning and is necessarily confined to only the high altitude eruption cloud. Subsequent GOES images were taken at 30 minute intervals. Thus the GOES photographs have proven of primary value for tracking the motion of the high altitude ash cloud, since they can yield few details about the early eruptive sequence itself.

The May 18th eruption was also detected by infrared sensors aboard two U. S. Air Force satellites. View angles are similar to those of the GOES-East

and GOES-West weather satellites. Essentially continuous data are available following the initial sighting of the eruption plume at 15:32:57 UT. It appears that the completeness of the data base is unique, particularly during the early stages of the eruption. Dual monitoring permits triangulation so that both the horizontal and vertical development of the eruption can be determined with good temporal resolution. Successful triangulation depends on identifying common points in the data from both satellites; this is not always possible, but can usually be achieved with the highest plumes and with the sensible periphery at the southern, eastern and northeastern limits of the cloud. Because the cloud is viewed from an angle relative to the local vertical, placing a given observed feature in its correct location on a latitude-longitude grid depends on knowledge of the altitude of the feature. This includes in particular the periphery of the cloud as a whole. This requirement is also true, of course, of the GOES images and, to a lesser extent, of the single NOAA-6 photograph made at 16:54 UT.

In the short-wavelength infrared spectral region employed by these sensors, the ash cloud can be seen as the result of scattered solar radiation provided that atmospheric attenuation is not so great as to obscure the cloud. Solar scatter was certainly the dominant source of the observed signal when the cloud was at high altitude and relatively cool. On the other hand, during much of the early development of the eruption the hot cloud at or near ground level could be seen in self-emission. This was also true at later times whenever the ash cloud configuration at higher altitude was such that the sensors could view down to the crater and thus see material being expelled directly. Derivation of a surface temperature for the cloud depends however on various assumptions which will be discussed later.

In this report the emphasis is on the time between the beginning of the eruption and the first GOES photograph at 15:45 UT, since the principal features of the eruption appear to have been established by this latter time. Later data will be presented when they have a bearing on interpreting the early-time events.

Figure 1 shows a schematic map of the area around Mt. St. Helens showing some significant landmarks which will be referred to later in the text. Prior to the May 18th eruption the summit of Mt. St. Helens had an altitude of 2948 meters, and was located at 46.20°N, 122.18°W (geographic coordinates will be quoted as decimal fractions of degrees throughout this report in order to facilitate distance comparisons). Spirit Lake lies north and slightly east of Mt. St. Helens; the Toutle River flows westward from the south end of Spirit Lake and eventually empties into the Cowlitz River just before the latter joins the Columbia. Mt. St. Helens lies on the western side of the Cascade Range; the largest of the nearby mountains are to the north and east. Mt. Margaret, at 1786 meters, lies directly north; Elk Rock, the highest of the mountains defining the Toutle River valley to the west, is only 1338 meters high. Figure 1 also shows the extent of the destruction zone other than just tephra fall or flooding based on maps produced by the U. S. Geological Survey. This map can be used with several figures in other sections to locate the areas of principal impact for specific "events" during the eruption sequence.

15:32:00 - 15:34:30 UT - THE BEGINNING

The earthquake which apparently triggered the eruption occurred shortly after 15:32 UT. The first satellite observation was made at 15:32:57 UT. The subsequent history of the observed intensity and vertical and lateral develop-

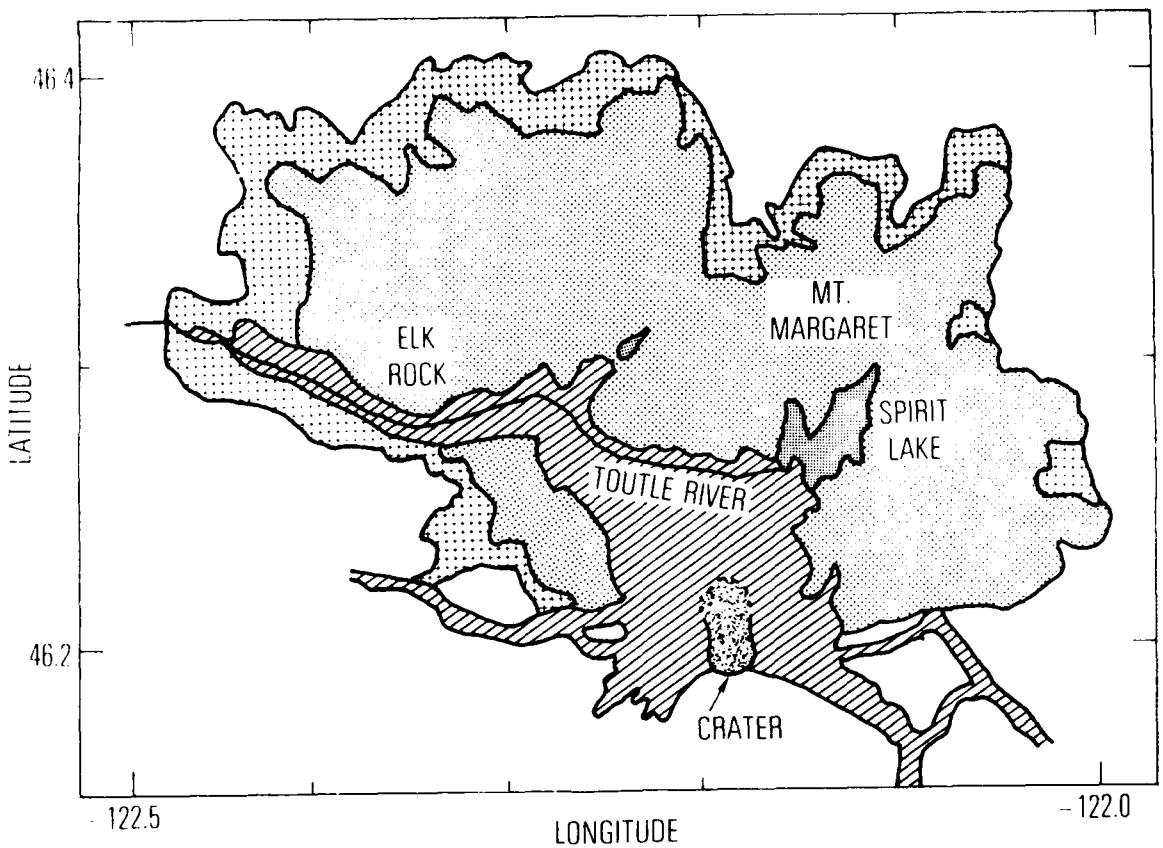

Figure 1. Map of the area surrounding Mt. St. Helens. The extent of various types of damage as determined by the U.S. Geological Survey is indicated by the shading: heavy stippling: new lake and new lake elevation; light stippling: downed timber; cross-hatching: major mud slides; square-hatching: damaged timber.

ment is given in Figures 2-4. (The latitude/longitude values plotted in Figure 4 assume an altitude of 6000 ft above mean sea level - about midway between the peak and base of the mountain. For material above that level the primary effect is an apparent northward shift approximately 1.25 times the altitude difference.) The altitude cannot be determined directly immediately following the first sighting but the location and low intensity of the returns indicate that the material was at relatively low altitude. The first detection of hot material was made at about 15:33:10 UT after which triangulation was at least intermittently possible. The subsequent rapid fluctuations in the observed intensity were tracked by both satellite sensors. The fluctuations may have resulted from a series of perhaps 3 (or more) essentially vertical emissions of material of differing temperature. Triangulation during this period gives a plume top varying between 3 and 6 km. It is difficult to assess whether the plotted peak altitude variations represent the true instantaneous values for the entire cloud; each of the 3 individual segments corresponds to a maximum in the intensity curve and could give the peak altitude of individual emission "events". Whatever the case, the peak altitude certainly stays below 6 km prior to 15:34:30 UT.

During this period the only significant lateral motion was toward the east and northeast. The apparent northward motion need not have extended much beyond the northern base of the mountain at 46.26°N; the additional 0.04° (~ 4 1/2 km) apparent in Figure 4 could have arisen from a projection effect caused by the cloud peak being at ~5.5 km. Two lines delineate the eastern periphery in Figure 4. The continuous (upper) line is the boundary of higher intensity returns which was a well defined region; the lower line locates a series of low intensity returns. The latter was an expanding cloud of apparently relatively low temperature material (seen in reflected light) moving eastward at

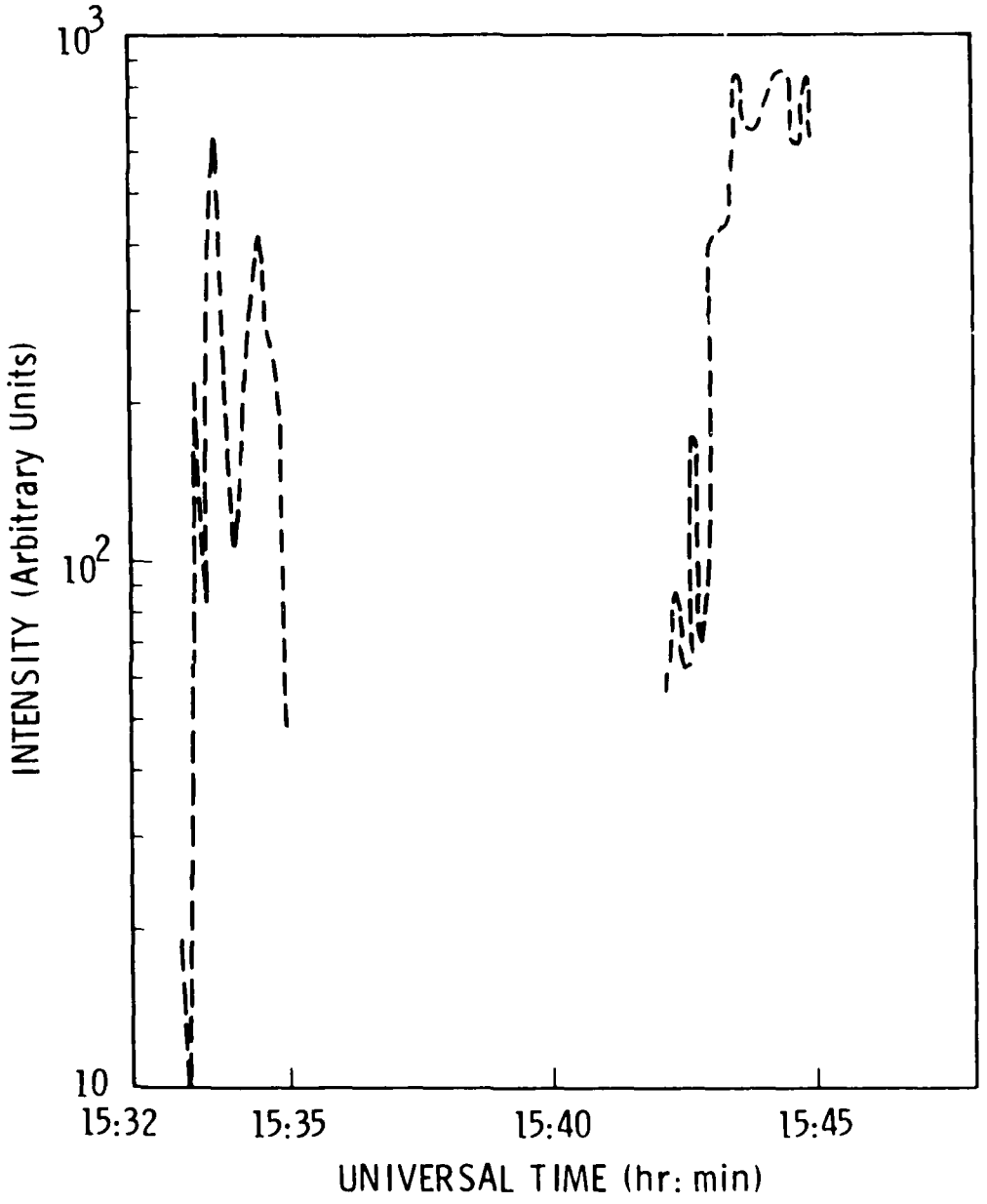

Figure 2. Measured SWIR intensity as a function of time near the crater of Mt. St. Helens.

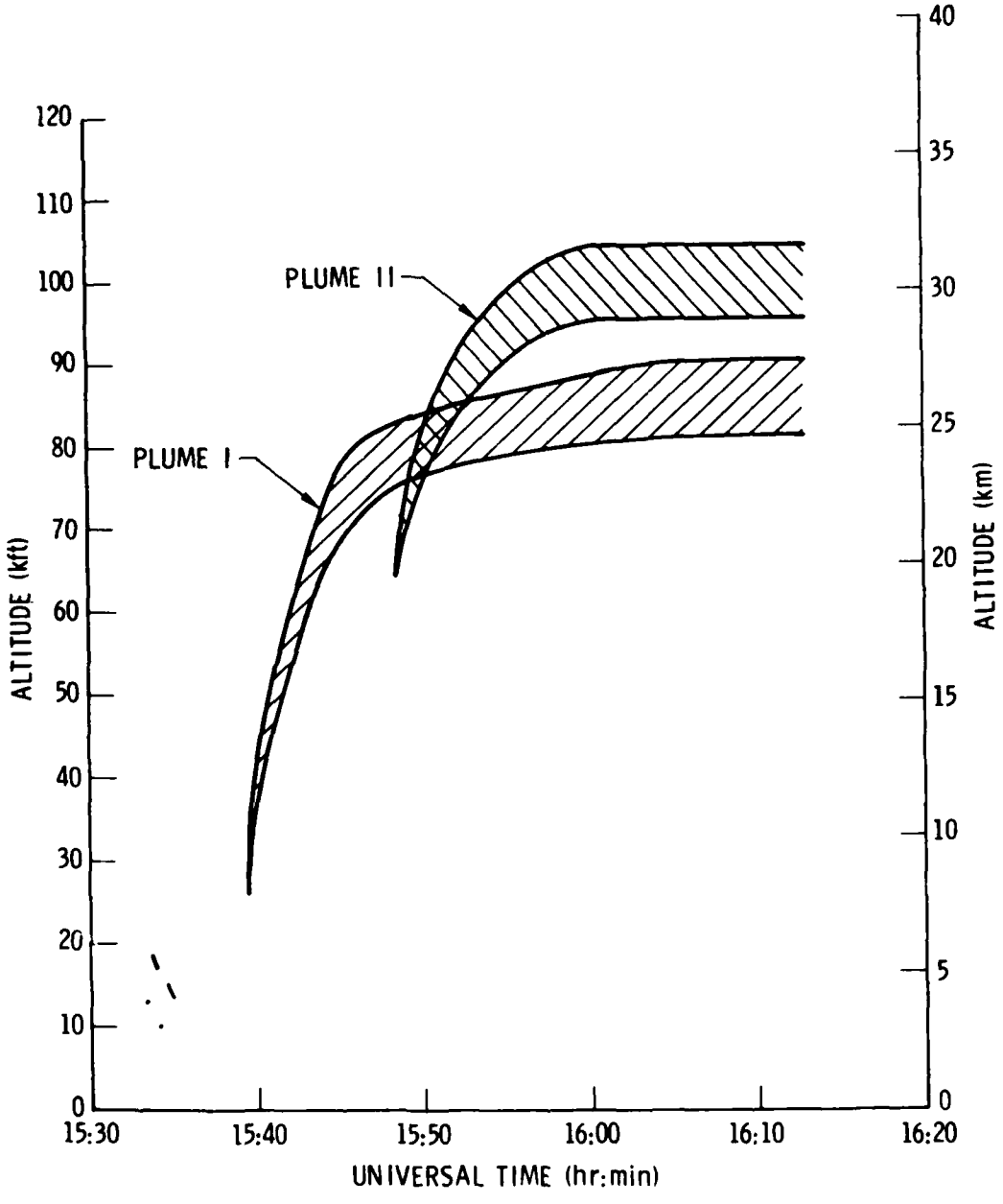

Figure 3. Peak altitude of the ash plumes based on triangulation.

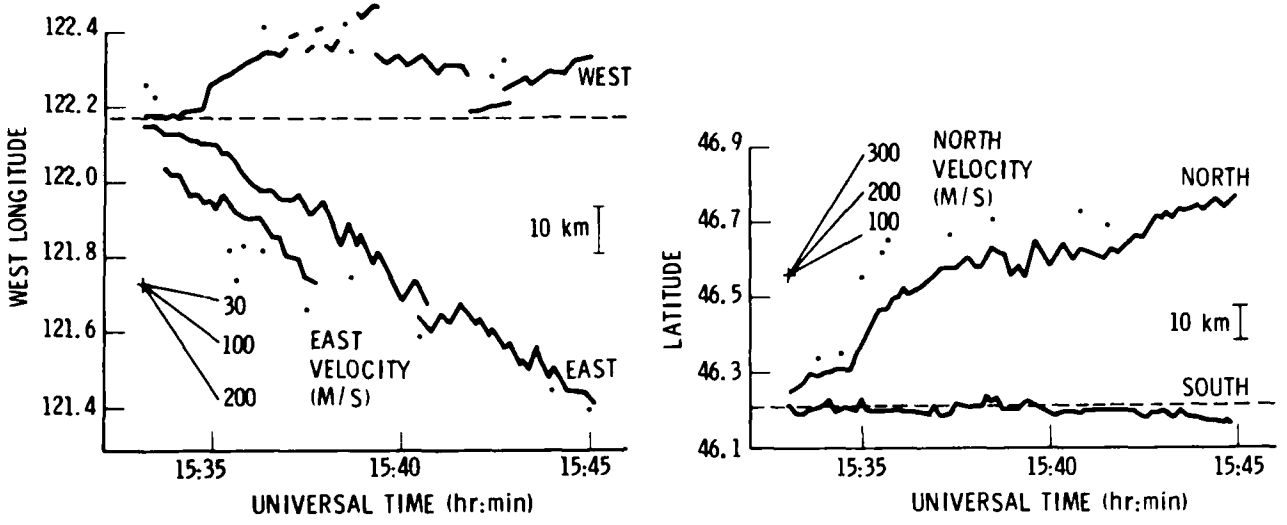

Figure 4. Location of the observed limits in latitude and longitude of the expanding ash cloud as a function of time. The ash cloud is located between the plotted lines. The nominal location of the peak of Mt. St. Helens (46.20°N, 122.18°W) is indicated by dashed lines. The mountain is approximately 8 km in diameter at its base. The eastern edge is given by two curves, corresponding to two well-defined boundaries. The lower of the two is a series of relatively low intensity returns which eventually fade into the background; the upper curve begins as high intensity returns which gradually decrease but remain distinct. Isolated single returns may indicate the presence of ash or they may be background. The insets give slopes corresponding to various values of velocity. Note that the plotted locations assume a constant altitude of 6000 ft; the effect of vertical displacements is discussed in the text.

about 100-110 m/sec (220-250 mph). Extrapolating backward indicates that the material began its motion away from the mountain shortly after 15:32:00 UT. This was the cloud which rapidly enveloped witnesses to the northeast. The cloud reached Bear Meadow, for example, at about 15:33:30 UT; this time corresponds closely to the estimate made by Keith Ronnholm that 90 seconds had elapsed since the beginning of the eruption when the cloud reached his location at Bear Meadow. This was the material ejected immediately following the original avalanche; a speed of approximately this magnitude has been derived from sequencing of still photographs (Voight et al., 1980). Meanwhile the eastern boundary of the main (hot) mass of material was moving eastward at 30-40 m/sec, which is only about twice the rate which would arise from just the prevailing westerly winds below 6 km. At 15:34:30 UT this hot mass was about 6 km wide, from east to west. Thus, although a great deal of hot material may have been ejected in the 2-1/2 minutes since the eruption began, up to this point the major part had been confined to the northern face and the southern sections of the Spirit Lake area. This mass of material had probably risen to a somewhat higher altitude than the more easterly cooler section.

Estimating the temperature from the measured intensity is not a straightforward procedure. Although the solar scattering contribution is certainly negligible (< .05 times the peak recorded intensity), other factors, such as atmospheric transmittance, emissivity, and actual source dimensions, are more difficult to determine. Internal evidence in the data as a whole indicates that the major part of the atmospheric absorption took place in a "haze" layer at roughly 10 km altitude. Because of this haze layer, calculated transmission curves based on atmospheric soundings are clearly much too high. The atmospheric transmittance was determined therefore by utilizing the relative intensity seen by the two sensors viewing at very different zenith angles (and

hence different path lengths) to select for internal consistency among a range of calculated transmittance profiles. Utilizing this transmittance, the peak measured intensity corresponds to a temperature of 450-500K; the considerations above, taken together with the fact that this value applies to the surface of the ash cloud, would indicate that this is a lower limit for internal temperatures.

15:34:30 - 15:38:50 UT - THE SURGE

At about 15:34:40 UT the character of the eruption changed dramatically. The hot material which had been confined to the north face of Mt. St. Helens appeared to suddenly split and began to move east and west (Figure 5), while at the same time an arcuate mass appeared at the northern periphery moving rapidly outward (Figure 6). Within seconds the peak intensity measured at the volcano itself fell rapidly and soon disappeared into the background. This period was the principal destructive surge, or blast. Each of these phenomena will be examined individually.

The westward and northward surges can be readily identified in Figure 4, where are plotted the most easterly, westerly, northerly and southerly points on the boundary. Because the prevailing westerlies have already blown the cloud top to the east, the virtually instantaneous expansion in that direction is masked when displayed in this fashion. The satellite view angle did permit seeing down to the ground along the southern periphery so that the expansion there can be readily followed. The approximate tracks and the location and intensity of the returns as a function of time are given in Figures 5 and 7. Note that in this case we are plotting the periphery of relatively high intensity returns (the intensity below which solar scattering is dominating the signal is ~30-40 in the arbitrary units plotted). The plotted intensity

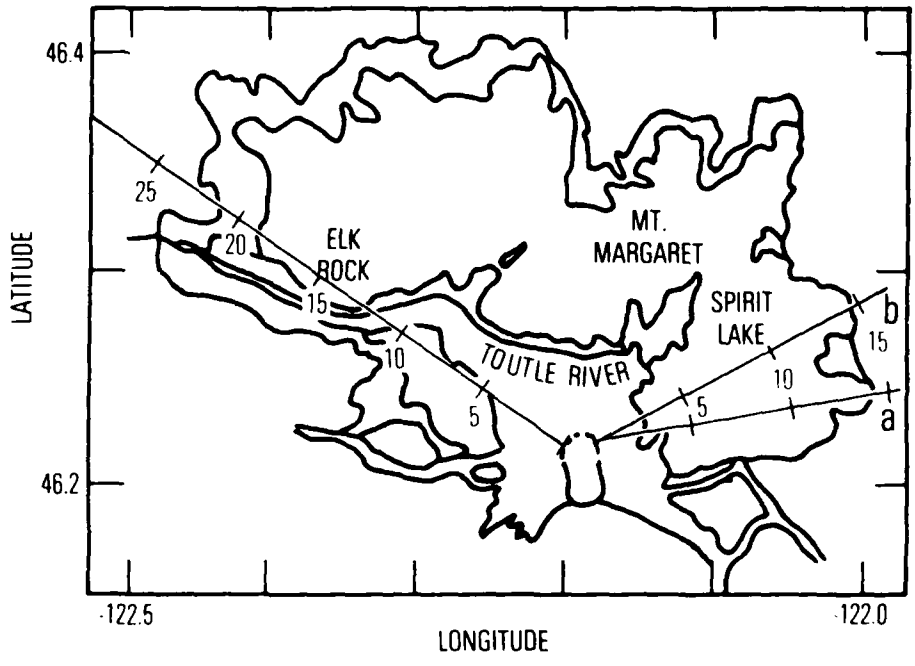

Figure 5. Approximate paths for the southern boundary of the eastward and westward surges. Tick marks are placed at 5-km intervals. The two eastward tracks labeled "a" and "b" are discussed in the text.

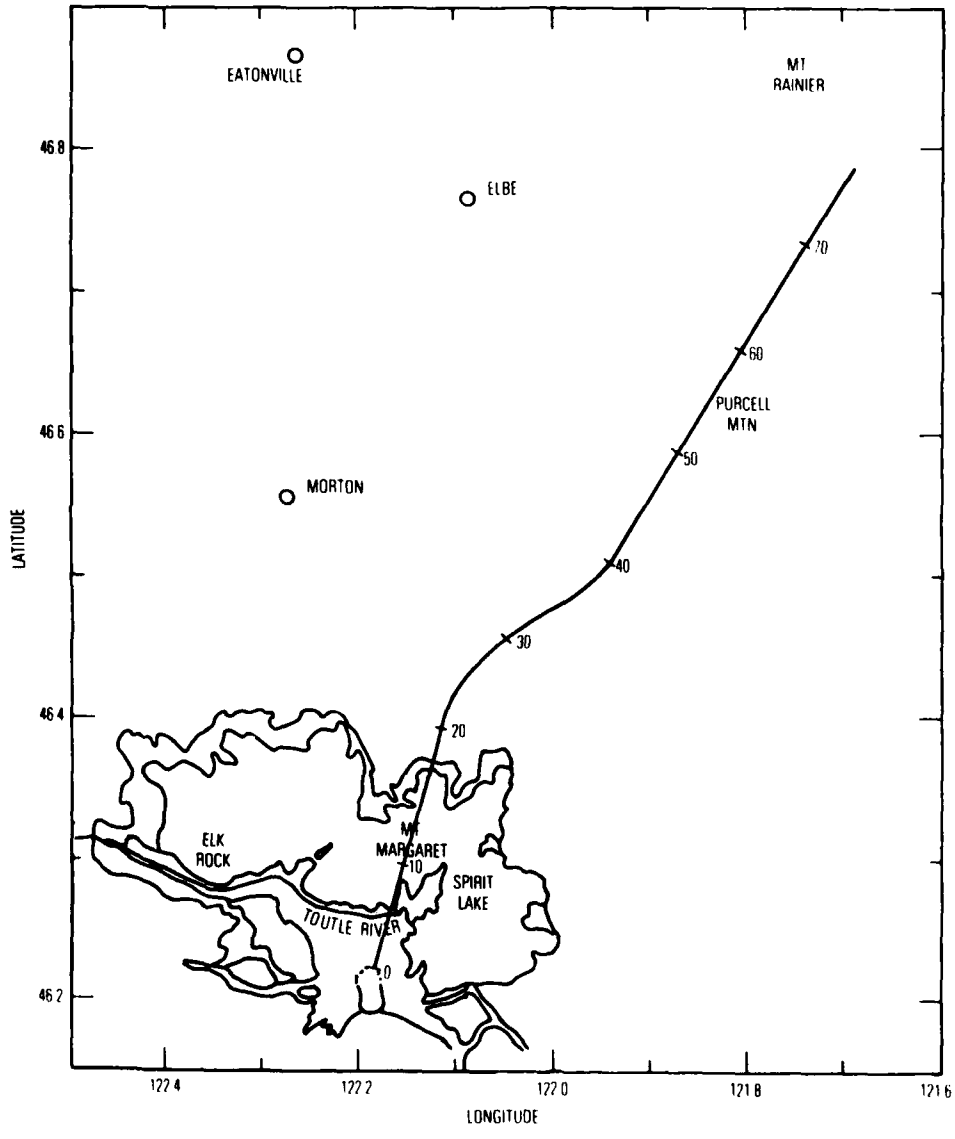

Figure 6. Approximate path followed by the northward surge. Tick marks have been placed at 10-km intervals.

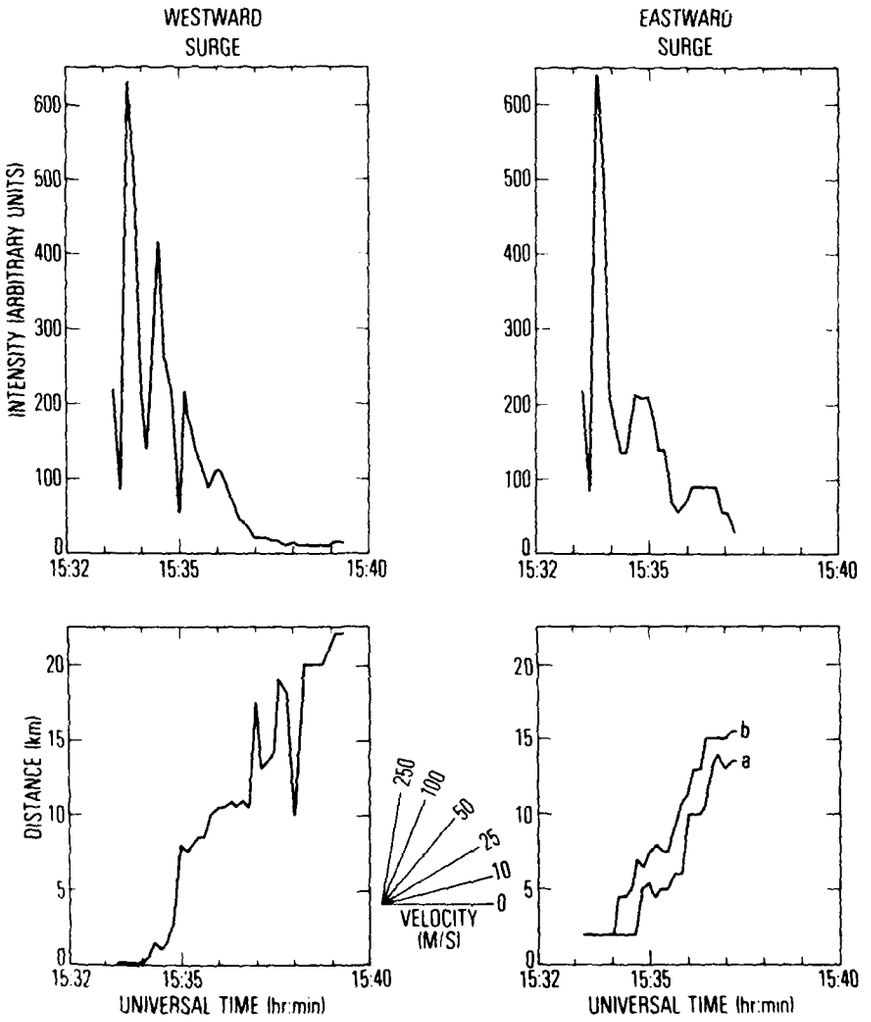

Figure 7. Intensity (upper graphs) and distance (lower graphs) for the eastward and westward surges as a function of time. The inset shows slopes corresponding to various values of velocity. Note that prior to about 15:34 UT only a single mass can be distinguished; hence the corresponding intensity readings are the same for both graphs.

represents the maximum value within an area around the leading edge small enough to be considered part of the advancing front (a few kilometers). Thus the maximum intensity plotted for the eastward and westward surges are identical up to 15:34:00 UT. The angles of the tracks are:

Westward: ~ 55° West of North

Eastward: ~ 80° East of North (labeled a)

Note that these tracks also define the southern boundary of the area of complete timber destruction, as can be seen by comparing with Figure 1. A second eastward track, labeled b, is also shown. Observations along track b may not be free of projection effects, i.e., coupling of vertical and horizontal motion; the measurements are given in Figure 7 because they indicate rapid motion somewhat earlier than it becomes evident along track a.

Immediately following 15:34 UT some westward expansion could be noted; it was slight and, based on the overall cloud behavior, may have represented a mushrooming at higher altitude. The first real "surge" occurred at about 15:34:45 UT and could be identified simultaneously both east and west. The initial surge carried the material from 3-5 km at velocities of 150-250 m/sec or greater. This was followed by a full minute of slow expansion (~ 40 m/sec) during which the intensity fell by more than a factor of 2. This relatively slow expansion continued on the west; the average peripheral velocity was ~45 m/sec between 15:34 and 15:39 UT, by which latter time the edge of the devastation zone had been reached. The intensity continued to fall, reaching solar scattering levels by about 15:37:00 UT. The scatter in locating the edge coincided with this drop in intensity. At the eastern edge, in contrast, two subsequent "surges" appear to have occurred, one at about 15:35:50 UT, the

other about 40 seconds later; in each case the inferred velocity was between 250 and 400 m/sec. It is possible that these two surges are not truly distinct events, but even simple averaging gives a velocity of 140 m/sec between 15:35:50 and 15:36:40 UT. By this latter time the eastern edge of the devastation zone had been reached, and subsequent intensities and expansion rates remained small.

The path of the northward surge is given in Figure 6. The observed intensity was at all times relatively low, corresponding to values for scattering of incident solar radiation. This implies that the material was relatively cool (< 400K) and/or relatively dispersed. The former was probably true at all times; the latter was certainly true after 15:39 UT when the material was at high altitude. This conclusion is based on the fact that only one of the satellite sensors could reliably detect this plume at any given time, specifically that sensor which could view through the greatest depth, i.e., had an essentially edge-on view. As a result, reliable triangulation is not possible and the altitude profile given in Figure 8 is inferred based on internal characteristics of the data, for example, penetration of the haze layer at about 10 km and apparent motion relative to plumes I and II.

The northward surge drove material before it in a fan-shaped segment with an opening angle of between 40° and 50°. The initial direction of motion was about 15° east of north, hence this blast wedge extended from roughly 10° west of north to about 40° east of north. The distance of the periphery along this track as a function of time and the inferred velocity are given in Figure 8. There exists a timing difficulty with respect to coordinating the northward surge with those to the east and west. The first indication of the high velocity lateral expansion appeared in all three directions simultaneously, namely at 15:34:50 UT, yet the east and west surges could be followed from the moun-

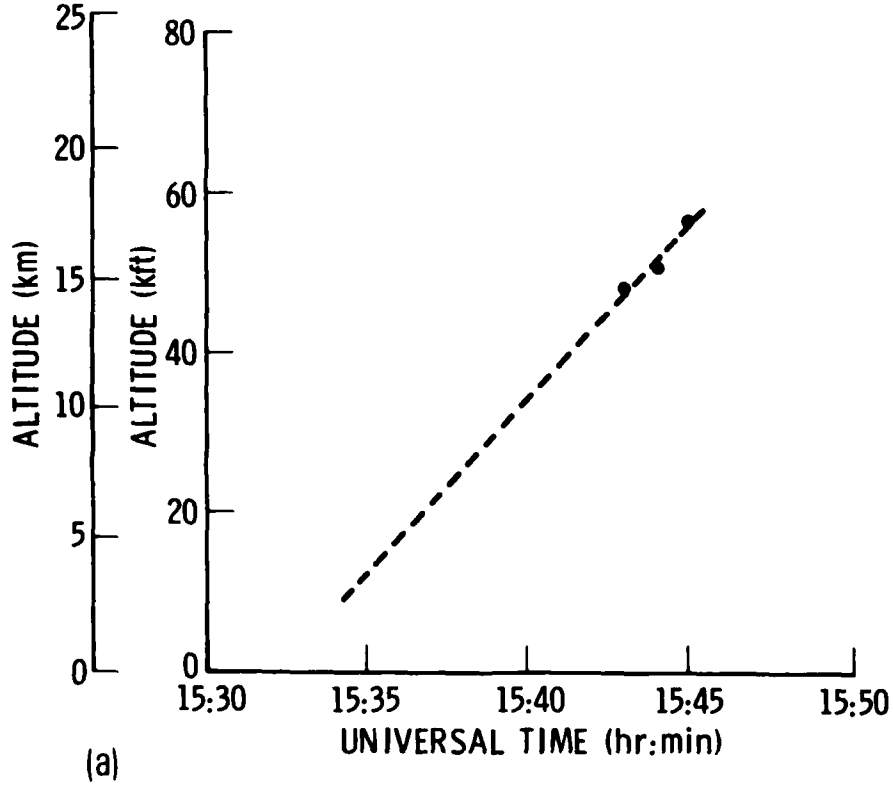

Figure 8(a). Altitude of the leading edge of the northward surge as a function of time. The plotted points, though not well determined, do indicate the general altitude range. The dotted line is a simple linear extrapolation backward in time.

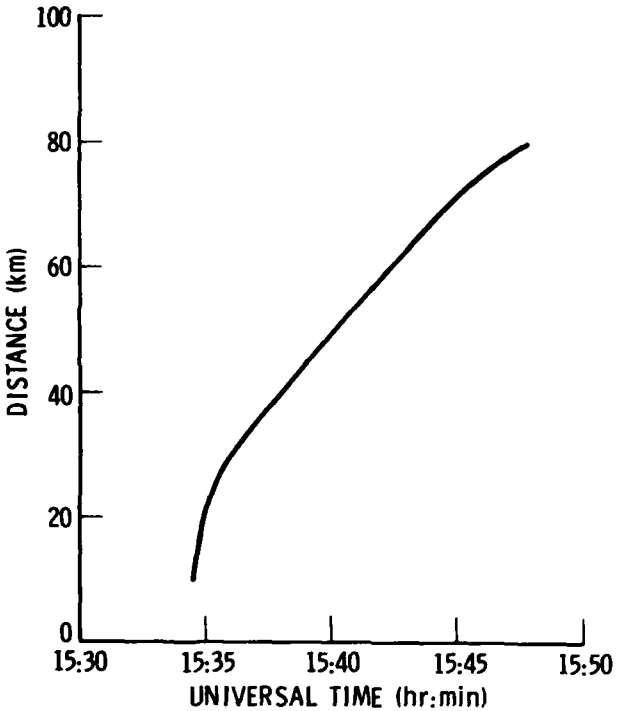

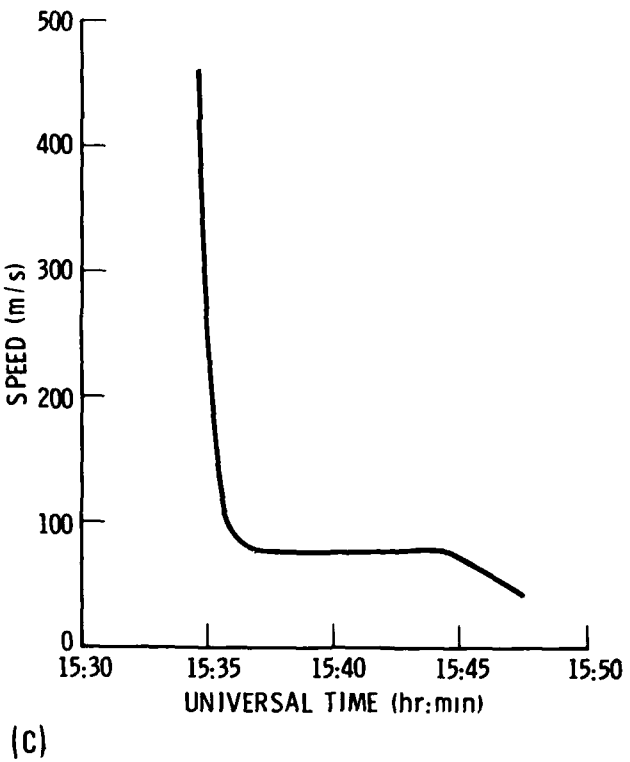

Figures 8(b) and (c). Distance (b) and speed (c) of the leading edge of the northward surge as a function of time along the path shown in Figure 6. The measured values have been considerably smoothed in deriving these curves and first-order corrections for the projection effect caused by the rise in altitude have been made.

tain itself whereas that to the north had to expand past pre-existing material, the northern edge of which was some 10 km north of the summit. Between 15:34:45 and 15:35:05 UT the average velocity along the northward track appears to have been ~450 m/sec (i.e., greater than sound speed!). Extrapolating backward at this velocity implies that the impulse at the mountain might have occurred at or before 15:34:20 UT. While this time does coincide with the last significant maximum in the intensity observed at the mountain, there is otherwise little to distinguish it from the times of the earlier maxima. In particular, there was no significant reaction in the east-west direction at that time.

The northward-moving surge reached the northern periphery of the devastation zone by 15:34:55 UT but continued to expand. There is a hint in the data that the moving section partially detached in some manner from the main body of material near this northern boundary. Given the low intensity of the source, however, such an interpretation is only tentative. As will be noted in a later section, the highest altitude plumes showed a configuration which may have mirrored this detachment.

15:38:50 - 15:45:00 UT - VERTICAL MOTIONS

Following the drop in intensity at 15:34:40 UT it is not possible to reliably triangulate for altitude anywhere on the developing ash cloud. Much of the signal attenuation was evidently occurring within an apparently relatively thin layer of haze located at about 10 km altitude. Thus the observed intensities remained essentially constant as the eruption plumes rose in the atmosphere. After breaking through the absorbing layer, however, the observed intensities rose rapidly and triangulation was possible once again. The first penetration occurred at 15:38:50 UT. At that time the vertical velocity was

about 40 m/sec (8000 ft/min). Extrapolating this value backwards gives a start time for the vertical rise of about 15:35 UT. This ash cloud thus began its rise essentially coincident with the major surge. The plume had a horizontal shape and area roughly that of the devastation zone and was, in fact, located essentially directly above that zone except for a slight eastward shift due to the westerly winds. Plume I eventually stabilized between 24 and 27 km (the quoted range is not the thickness of the cloud, but rather the scatter of the peak altitude determination).

Though somewhat out of order chronologically, it is appropriate to discuss at this point a second high altitude plume, labeled plume II in Figure 3, which followed plume I by about 6 minutes. In fact, plume II attained an even higher ultimate altitude, between 29 and 32 km, and was both larger and, apparently, denser than plume I. The initial geographical location (corrected for a wind-driven eastward shift) of plume II was considerably to the north and east of plume I and of the devastation zone. The two plumes at altitude can be seen well in the GOES-West photograph taken at 16:15 UT (Figure 9) though the lateral separation of the two clouds is exaggerated by the oblique viewing angle. This photograph will be discussed more fully later.

Because of the sensor view angles, it was not possible to unambiguously distinguish plume II from plume I until 15:49 UT when the former had already reached about 21 km. At this point the cloud was rising at about 40 m/s, i.e., the same speed as that determined earlier for plume I. Extrapolating this rise rate backward to the ground yields 15:41 UT for a starting time, though this should probably be taken as a lower limit since the rise rate was not sampled until the plume was relatively near the final stabilization altitude. Near 15:41 UT the ground area in question was hidden from both sensors by plume I and/or the obscuring cloud layer at 10 km. The only significant

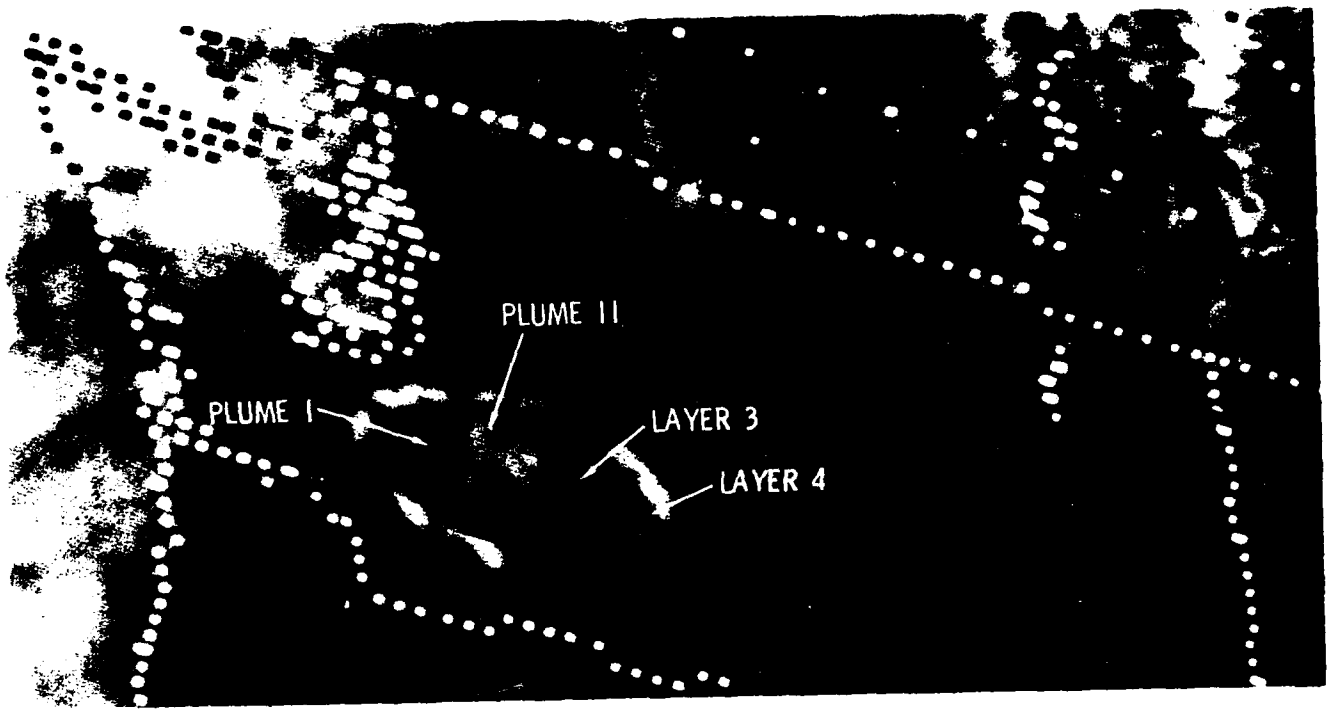

Figure 9. GOES-West visible image for the state of Washington for 16:15 UT, 18 May 1980.

"event" visible near this time occurred at the crater itself, 8-10 km to the south of the plume base, and thus appears to have had no direct connection to plume II. As shown in Figure 2 and previously discussed, the intensity at the crater fell rapidly at 15:35 UT and remained low; between 15:42 and 15:43 UT, however, the intensity there rose rapidly and soon attained a value greater than any measured during the initial eruptive sequence prior to 15:35 UT. This new ejection of hot material appears to have been vertical and doubtless corresponded to the establishment of the Plinian column which dominated the later eruption period. Although the motion of overlying ash clouds occasionally blocked the sensor line of sight for short periods, this column could be monitored for several hours thereafter.

In terms of total mass content, neither of the high altitude plumes represents a significant portion of the total material displaced by the eruption (~ 2 km^3) or even of that part which was removed as windborne ash (~ .2 km^3, according to Sarna-Wojcicki and Waitt, 1980). In fact, these plumes are only two of at least four readily identifiable ash clouds which were produced within the first 10-15 minutes. The four layers can be distinguished in the GOES-West visible image made at 16:15 UT (Figure 9). The high-altitude plumes I and II appear white in this image. At these altitudes (25-32 km) the winds were light; as a result these two plumes showed internal motion and some expansion but no significant lateral motion as a body, as can be seen in subsequent GOES-West images. It is possible to interpret the two high altitude plumes in two ways. On the one hand, the tephra in plumes I and II, particularly the former, may have been material carried out of the crater throat by the expanding gases which subsequently produced the shock front. Alternatively, this front may have carried little solid material as it emerged but rather drove forward (or forced aside) the great amount of ash which had

been evolved during the first 2 1/2 minutes of the eruption. In this view plume I is the vertically moving analog of the eastward and westward surges discussed in the previous section. Plume II then evolved out of the material transported to the north by the advancing shock front. The greater part of this earlier material appears to have been contained within a third layer which eventually stabilized at 18-21 km, moving toward the east at about 12 m/sec. For a variety of reasons, but principally the effect of the haze near 10 km, this ash layer could not be followed in detail throughout its early development. It could be observed reliably from both satellites only after about 15:48 UT, though it is possible to extrapolate features of its behavior to earlier times.

The fourth layer stabilized between 12 and 15 km altitude and appears to have carried the greater bulk of the tephra emitted at early times. This layer was produced by the Plinian column established after 15:42 UT, and hence probably contained a higher proportion of juvenile ash. This tephra was carried to the east at about 31 m/sec. The bulk of this ash cloud lay above the maximum winds which were about 33-35 m/sec at or somewhat below 12 km altitude. The heavier material falling out of this layer was thus blown ahead in a thinner curtain, an effect which can be seen in Figure 9.

SUMMARY AND CONCLUSIONS

The timing of the principal "events" discussed in this report is summarized in Table 1. The early eruption period was characterized by a complex sequence of emissions which began with the earthquake-triggered landslide at about 15:32 UT. During the first 2 1/2 minutes a great mass of material was evolved, most of which was confined to low altitudes above the northern face of the mountain and the area immediately to the north and east. The maximum velocity measured during this period was about 100 m/s toward the east and northeast. The principal destructive surge began at 15:34:50 UT, producing northward directed velocities in excess of sound speed (up to 450 m/sec) for a period of something less than a minute. The two highest plumes were produced by this event and therefore consist of ash evolved during the earliest times. Because of its high altitude, this material may have settled out very late, perhaps even after the major part of the eruption was over. Furthermore, the low winds obtaining at altitude would not have carried the plumes very far from the region of Mt. St. Helens during the intervening period. This early material may thus have settled out as a layer near or at the top of the tephra deposit. The Plinian column which was the dominant feature of the later period of the eruption was established between 15:42 and 15:43 UT. The ash plumes resulting from this early activity were still rising and evolving when GOES-West produced its first image at 15:45 UT, but by the time of the next photograph at 16:15 UT the principal high altitude layers had been established, and subsequent images show primarily its wind-driven evolution.

Table 1. Early chronology

Universal Time	Event
15:32	Magnitude 5.3 earthquake
15:32:57	First satellite observation
15:33:10	First emission of "hot" material - remains below 6 km
15:34:50	Major lateral blast to NNE - 350-450 m/s
15:36:00	End of explosive blast phase
15:39	Plume I penetrates 10 km altitude
15:42:10	Emission of hot ash from crater - establishment of Plinian column
15:50	Plume I near final altitude: 24-27 km
16:00	Plume II near final altitude: 29-32 km

REFERENCES

Voight, B., R. Janda, H. Glicken, P.M. Douglass, M. Nolan, and R. Hoblitt, Catastrophic Rockslide-Avalanche of May 18, 1980, Mount St. Helens Volcano, Washington, presentation made at the annual meeting of the Geological Society of America, 19 November 1980.

Sarna-Wojcicki, A.M., and R.B. Waitt, Areal Distribution, Thickness, and Composition of Volcanic Ash Erupted from Mount St. Helens on May 18, 1980, presentation made at the annual meeting of the Geological Society of America, 19 November 1980.

LABORATORY OPERATIONS

The Laboratory Operations of The Aerospace Corporation is conducting experimental and theoretical investigations necessary for the evaluation and application of scientific advances to new military concepts and systems. Versatility and flexibility have been developed to a high degree by the laboratory personnel in dealing with the many problems encountered in the Nation's rapidly developing space systems. Expertise in the latest scientific developments is vital to the accomplishment of tasks related to these problems. The laboratories that contribute to this research are:

Aerophysics Laboratory: Aerodynamics; fluid dynamics; plasmadynamics; chemical kinetics; engineering mechanics; flight dynamics; heat transfer; high-power gas lasers, continuous and pulsed, IR, visible, UV; laser physics; laser resonator optics; laser effects and countermeasures.

Chemistry and Physics Laboratory: Atmospheric reactions and optical backgrounds; radiative transfer and atmospheric transmission; thermal and state-specific reaction rates in rocket plumes; chemical thermodynamics and propulsion chemistry; laser isotope separation; chemistry and physics of particles; space environmental and contamination effects on spacecraft materials; lubrication; surface chemistry of insulators and conductors; cathode materials; sensor materials and sensor optics; applied laser spectroscopy; atomic frequency standards; pollution and toxic materials monitoring.

Electronics Research Laboratory: Electromagnetic theory and propagation phenomena; microwave and semiconductor devices and integrated circuits; quantum electronics, lasers, and electro-optics; communication sciences, applied electronics, superconducting and electronic device physics; millimeter-wave and far-infrared technology.

Materials Sciences Laboratory: Development of new materials; composite materials; graphite and ceramics; polymeric materials; weapons effects and hardened materials; materials for electronic devices; dimensionally stable materials; chemical and structural analyses; stress corrosion; fatigue of metals.

Space Sciences Laboratory: Atmospheric and ionospheric physics, radiation from the atmosphere, density and composition of the atmosphere, aurorae and airglow; magnetospheric physics, cosmic rays, generation and propagation of plasma waves in the magnetosphere; solar physics, x-ray astronomy; the effects of nuclear explosions, magnetic storms, and solar activity on the earth's atmosphere, ionosphere, and magnetosphere; the effects of optical, electromagnetic, and particulate radiations in space on space systems.

. . .


DAT
ILM